The Chromospheric Field Probed by the He I 10830 Line

Some Recent Developments

Andreas Lagg

Max-Planck-Institut für Sonnensystemforschung
Göttingen, Germany

Coupling and Dynamics of the Solar Atmosphere
Pune, India
Nov-11 2014

The He I atom (Centeno et al., 2008)

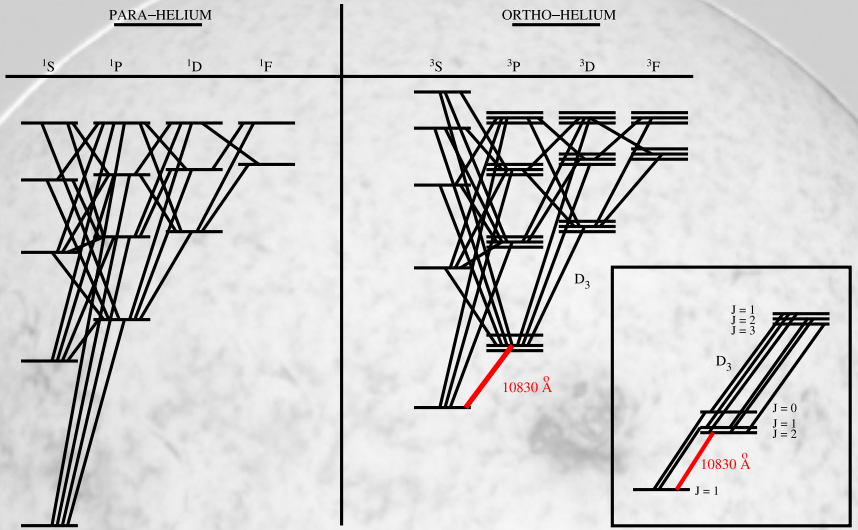

Coronal Illumination - Ionization - Recombination (Centeno et al., 2008)

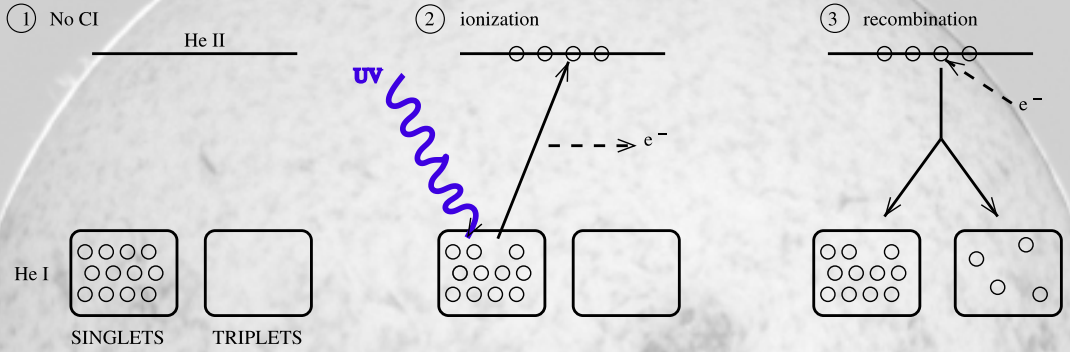

He I – What can be observed?

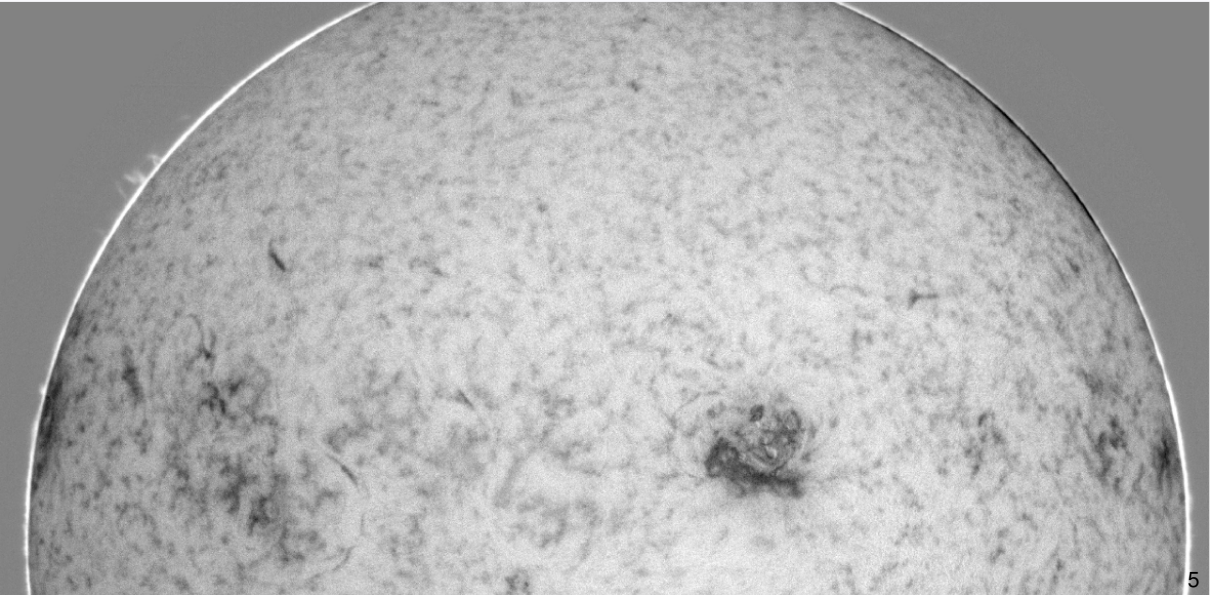

He I – Formation Height

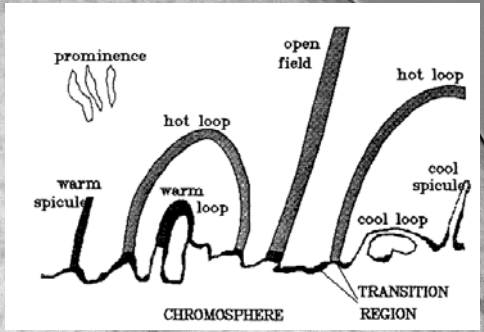

Avrett et al. (1994)

He I – Formation Height

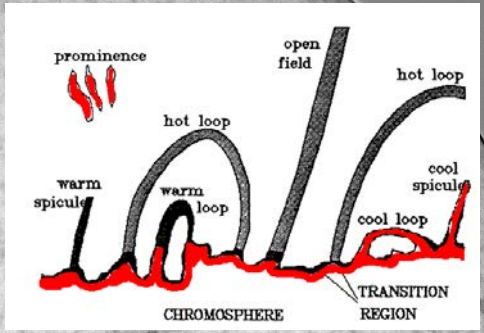

Avrett et al. (1994)

He I – Formation Height

Poster on He D3 results:

T. E. L. Libbrecht et al.:
Spectrographic Helium D3 observations with SST/TRIPPEL

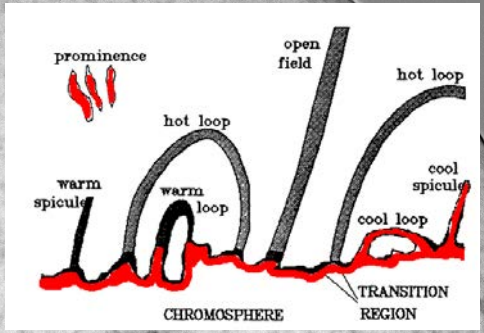

Avrett et al. (1994)

B-Field and He I 10830 Å

Zeeman + PB effect

- reliable magnetic field information for B$>$ 200 G
- simultaneous observation of photosphere (Si, Ca) and chromosphere (He)
- three (blended) HeI lines: (”blue” line + 2 ”red” lines)
- Paschen-Back effect for stronger fields

Hanle effect

- sensitive regime: ≈0.1–8 G
- saturated regime (8–100 G): directional information

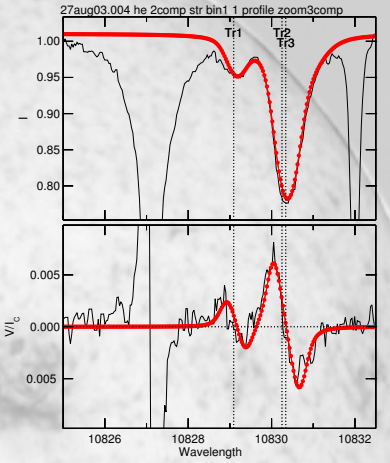

He I Observatories

He I 10830 full disk instruments

- SOLIS VSM and FDP
  (NSO; until 2014: Kitt Peak, 2014: Tucson: 2015: ???; Keller et al., 2003)
- Chrotel
  (KIS; Tenerife; Bethge et al., 2011)
- CHIP
  (MacQueen et al., 1998)
- NAOJ Solar Flare Telescope
  (NAOJ; Hanaoka et al., 2011)

He I 10830 at high resolution

- TIP-1
  (IAC; Tenerife; Martínez Pillet et al., 1999; Collados et al., 1999)
- TIP-2
  (IAC/MPS; Tenerife; Collados et al., 2007)
- ProMag (prominences)
  (NSO; Sunspot; Elmore et al., 2008)

Recent hi-res Spectropolarimeters

- FIRS, SPINOR, NIRIS, GRIS

Recent Hi-Res Spectropolarimeters

SPINOR @ DST (Sac Peak)

Socas-Navarro et al. (2006)

- full Stokes simultaneous obs. of several VIS + IR regions
- virtually any combination of spectral line

FIRS @ DST (Sac Peak)

Jaeggli et al. (2010); Schad (2013)

- 4-slit, dual-beam spectropol.
- Fe I 630.2 & He I 1083
- simultaneous with IBIS

NIRIS @ 1.6m NST (Big Bear)

Cao et al. (2012)

- attached to 1.6 m NST at Big Bear
- dual Fabry-Pérot Interferometers
- imaging polarimetry @ 0.″25

GRIS @ 1.5m GREGOR (Tenerife)

Collados et al. (2012)

- attached to 1.5 m GREGOR telescope (Tenerife)
- standard Czerny-Turner config.
- spectro-polarimetry @ 0.″25

The magnetic field configuration of a solar prominence inferred from spectropolarimetric observations in the He I 10830 Å triplet (Orozco Suárez et al., 2014)

quasi-horizontal solution

quasi-vertical solution

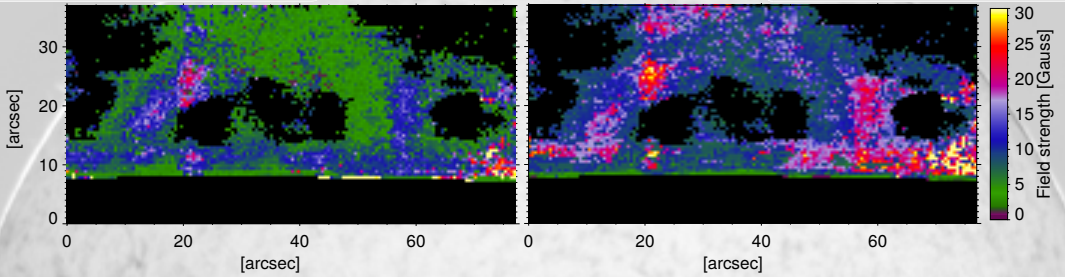

HAZEL inversions (Asensio Ramos et al., 2008)

70 s/slit pos

Ambiguities (unresolved, plausibility argument: use quasi-horizontal solution):

- Zeeman effect: 180° ambiguity
- Hanle effect: 90° and 180° ambiguity

The magnetic field configuration of a solar prominence inferred from spectropolarimetric observations in the He I 10830 Å triplet (Orozco Suárez et al., 2014)

quasi-horizontal solution

quasi-vertical solution

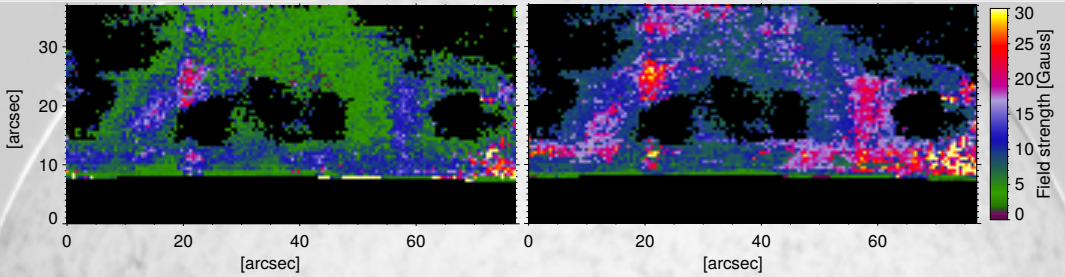

Magnetic field strength

- quiescent prominence, on average 7 G
- up to 30 G at prominence feet (coinciding with high opacity)

The magnetic field configuration of a solar prominence inferred from spectropolarimetric observations in the He I 10830 Å triplet (Orozco Suárez et al., 2014)

quasi-horizontal solution

quasi-vertical solution

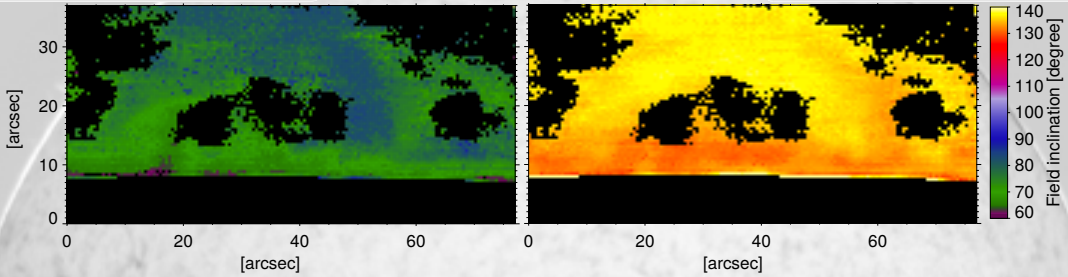

Magnetic field inclination

- inclined $\approx 77^\circ$ to solar vertical;
  in between previous results: 60° (e.g., Bommier et al., 1994) and horizontal (Casini et al., 2003)

The magnetic field configuration of a solar prominence inferred from spectropolarimetric observations in the He I 10830 Å triplet (Orozco Suárez et al., 2014)

quasi-horizontal solution

quasi-vertical solution

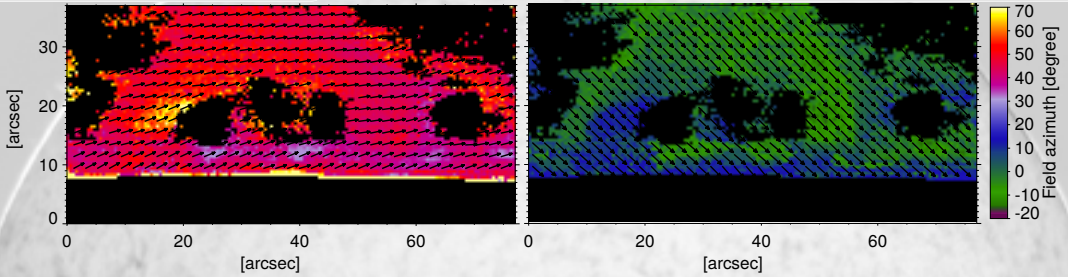

Magnetic field orientation wrt. prominence axis

- inclined $\approx 58^\circ$ / $\approx 156^\circ$ to prominence long axis (unresolved ambiguity), both solutions: inverse polarity prominence

He I Vector Magnetometry of Field-aligned Superpenumbral Fibrils (Schad et al., 2013)

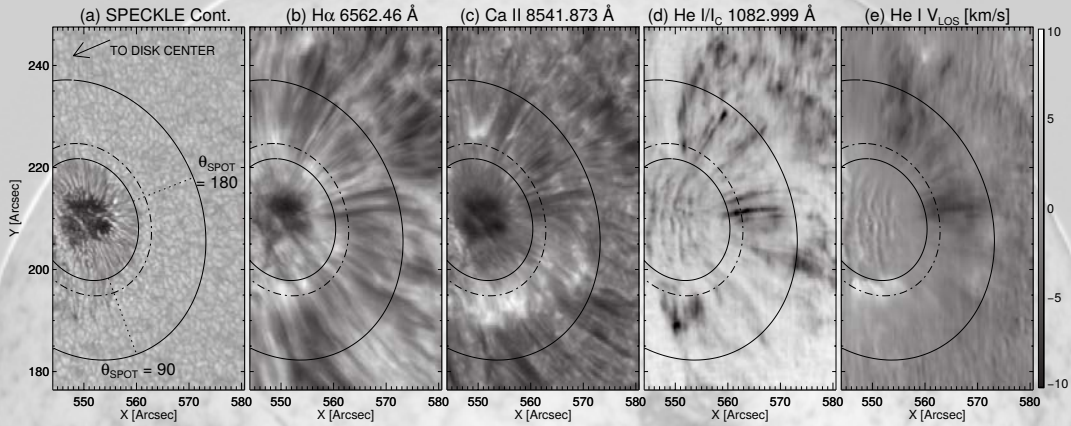

IBIS & FIRS Observations, NOAA AR 11408, Jan 29 2012, $\mu = 0.8$

He I Vector Magnetometry of Field-aligned Superpenumbral Fibrils (Schad et al., 2013)

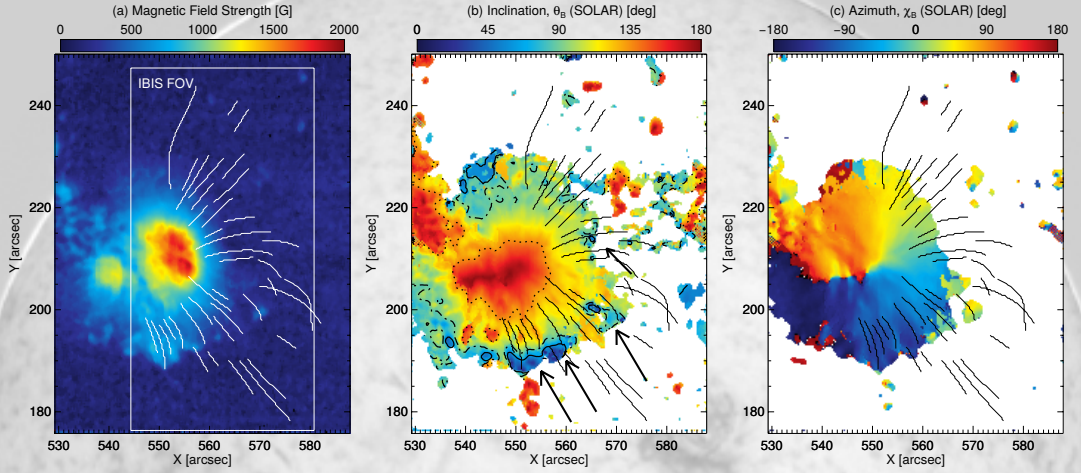

Photospheric field from Si I ME-inversions (HELIX$^+$ Lagg et al., 2009)

He I Vector Magnetometry of Field-aligned Superpenumbral Fibrils (Schad et al., 2013)

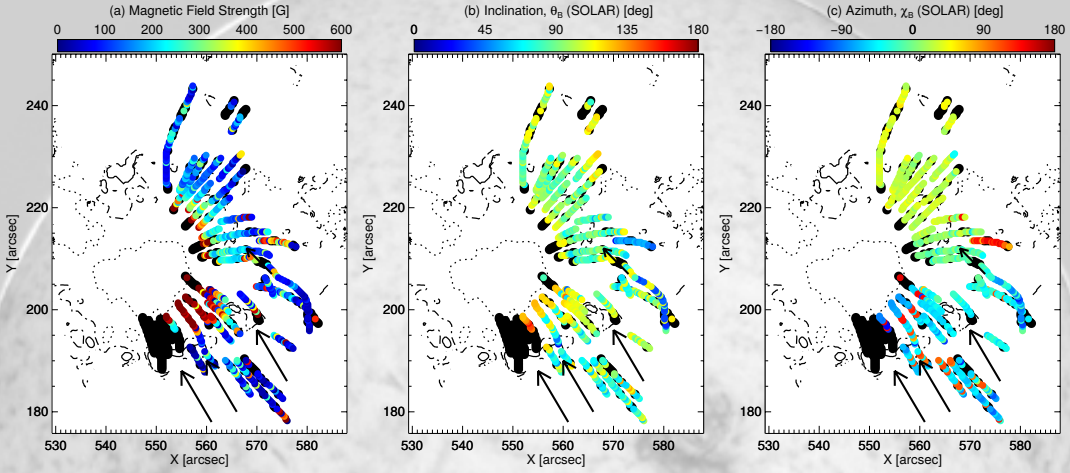

Fibril tracing (CRISPEX, Vissers & Rouppe van der Voort, 2012), careful disambiguation (Hanle & Zeeman), assumption on fibril height (1.75 Mm)

He I Vector Magnetometry of Field-aligned Superpenumbral Fibrils (Schad et al., 2013)

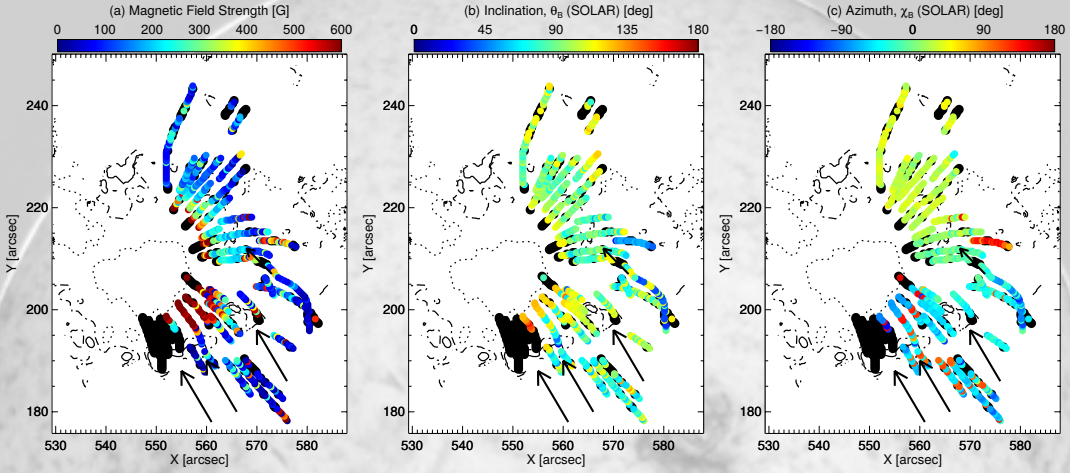

B-strength: rise in strength towards inner endpoints

He I Vector Magnetometry of Field-aligned Superpenumbral Fibrils (Schad et al., 2013)

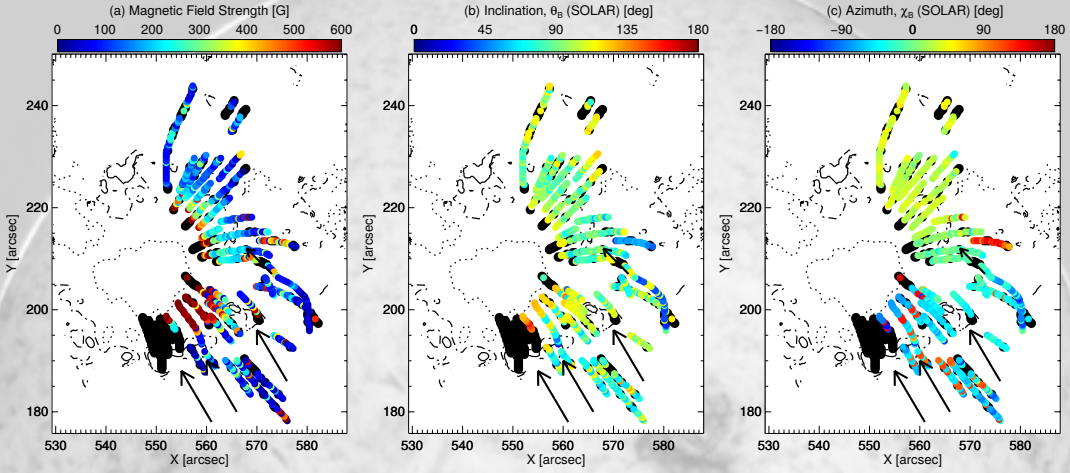

B-inclination: change at inner endpoint towards sunspot

He I Vector Magnetometry of Field-aligned Superpenumbral Fibrils (Schad et al., 2013)

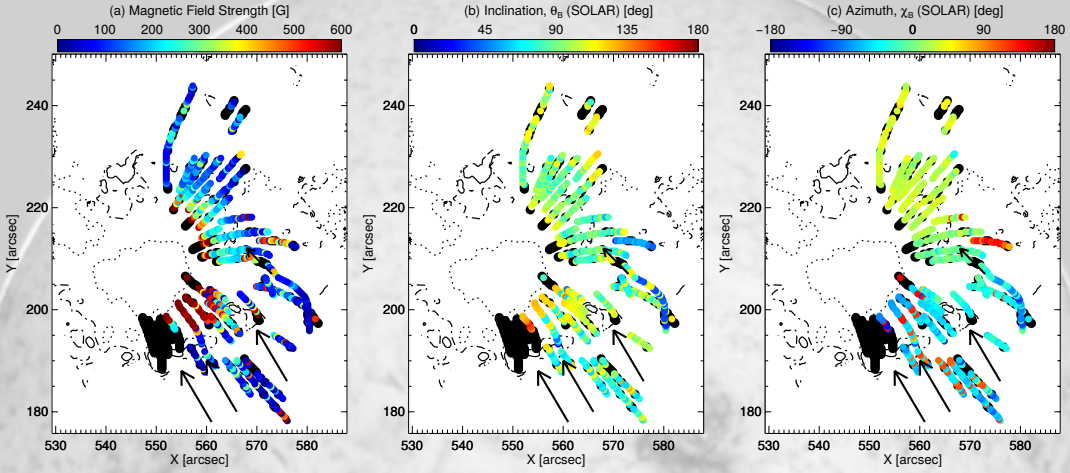

B-inclination: remain horizontal until outer endpoint
few fibrils: turn over again, connect in regions of opposite polarity photosphere

He I Vector Magnetometry of Field-aligned Superpenumbral Fibrils (Schad et al., 2013)

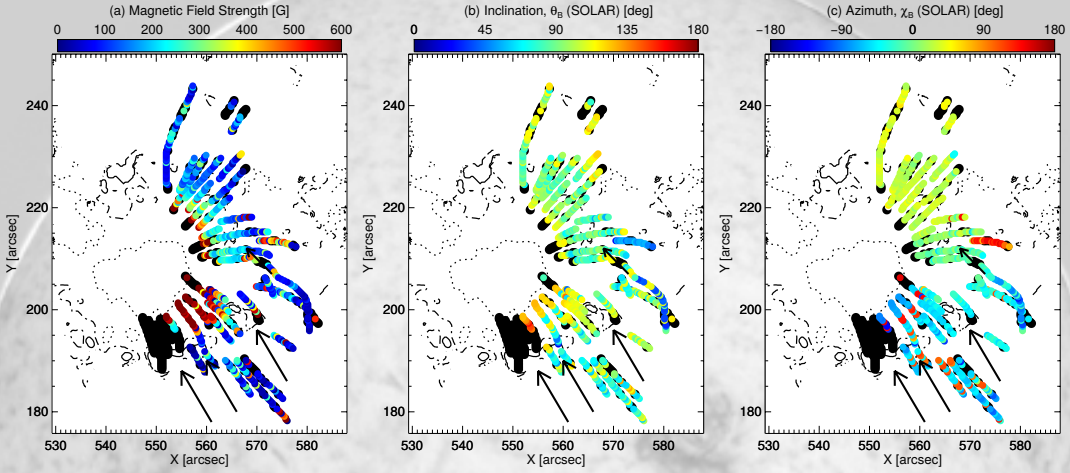

B-azimuth: aligned $\pm 10^\circ$ with fibrils

Multi-wavelength High-resolution Observations of a Small-scale Emerging Magnetic Flux Event and the Chromospheric and Coronal Response (Vargas Domínguez et al., 2014)

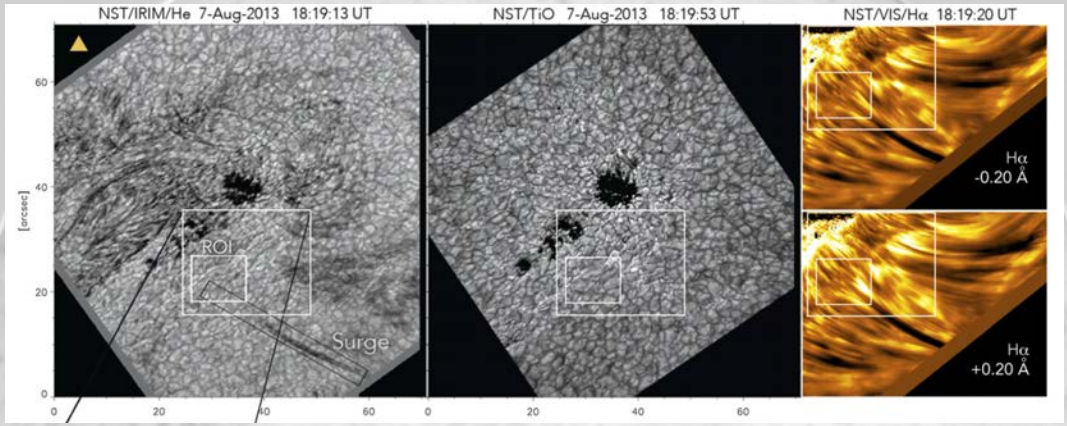

Multi-wavelength High-resolution Observations of a Small-scale Emerging Magnetic Flux Event and the Chromospheric and Coronal Response (Vargas Domínguez et al., 2014)

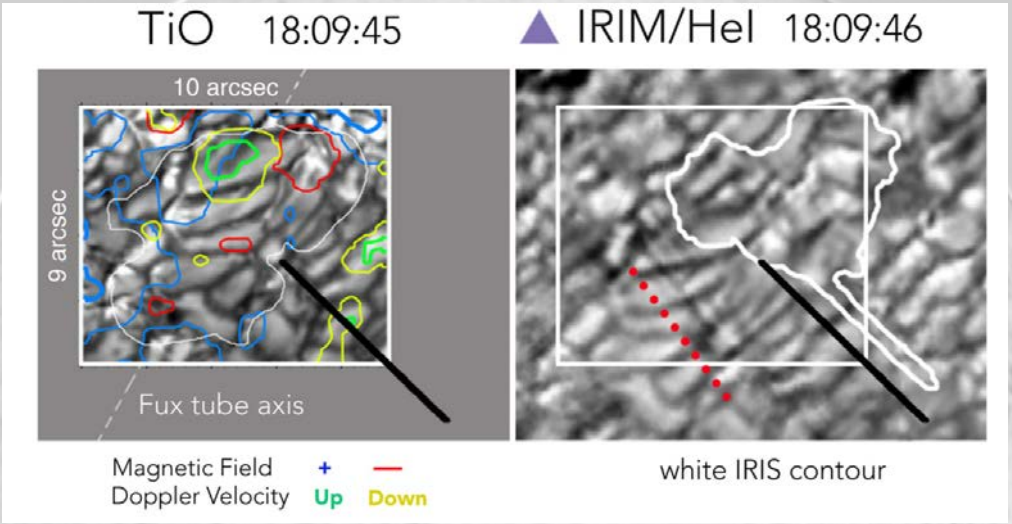

Multi-wavelength High-resolution Observations of a Small-scale Emerging Magnetic Flux Event and the Chromospheric and Coronal Response (Vargas Domínguez et al., 2014)

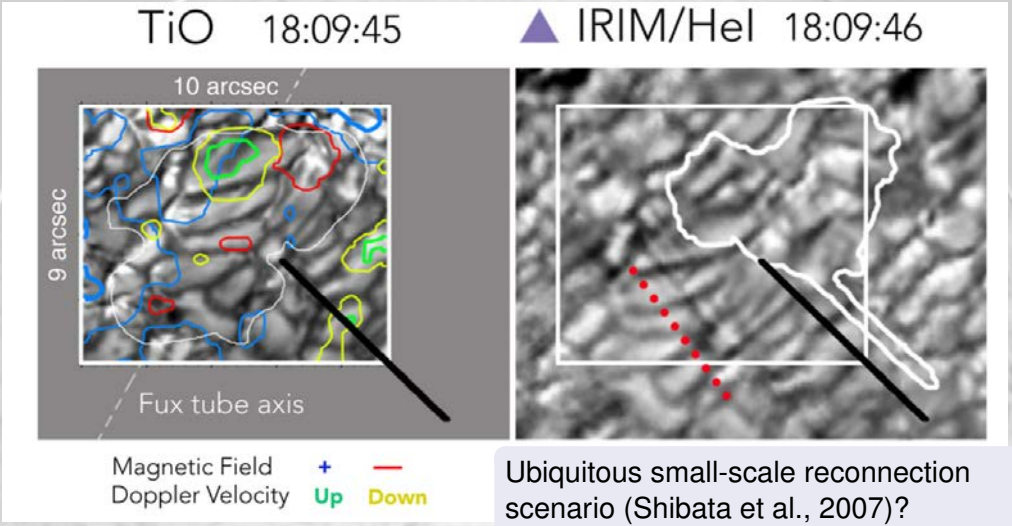

Ubiquitous small-scale reconnection scenario (Shibata et al., 2007)?

GREGOR/GRIS Data & First Results (June 2014)

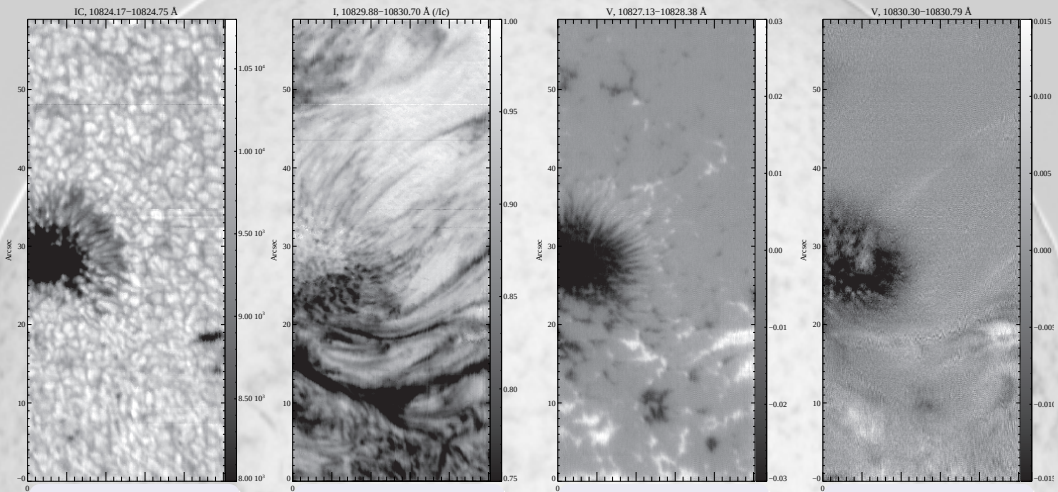

Stokes I_c | Stokes I_{He} | Stokes V_{Si} | Stokes V_{He}

GREGOR/GRIS Data & First Results (June 2014)

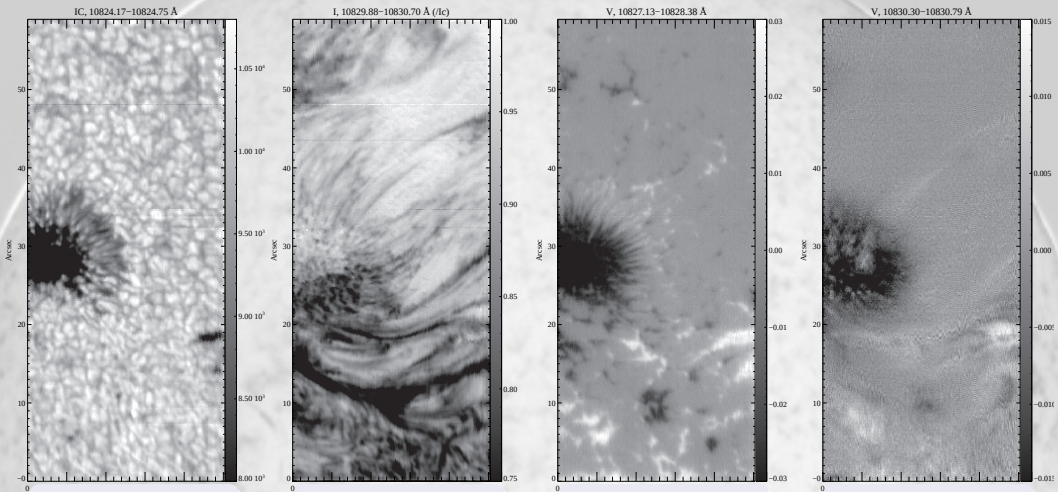

Stokes I_c | Stokes I_{He} | Stokes V_{Si} | Stokes V_{He}

GREGOR/GRIS Data & First Results (June 2014)

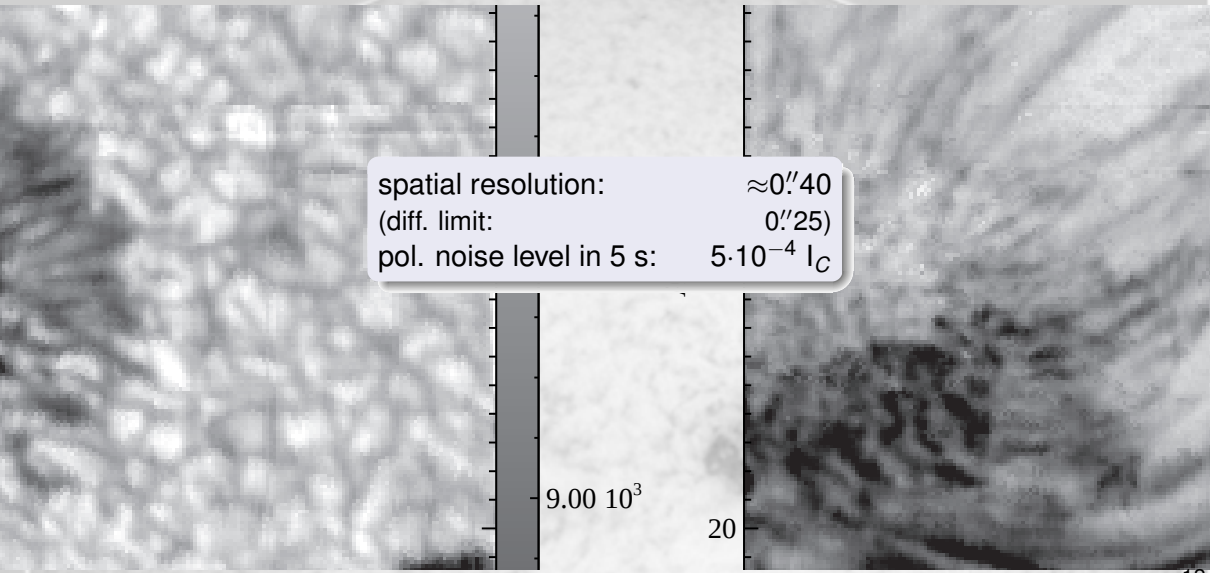

GREGOR/GRIS Data & First Results (June 2014)

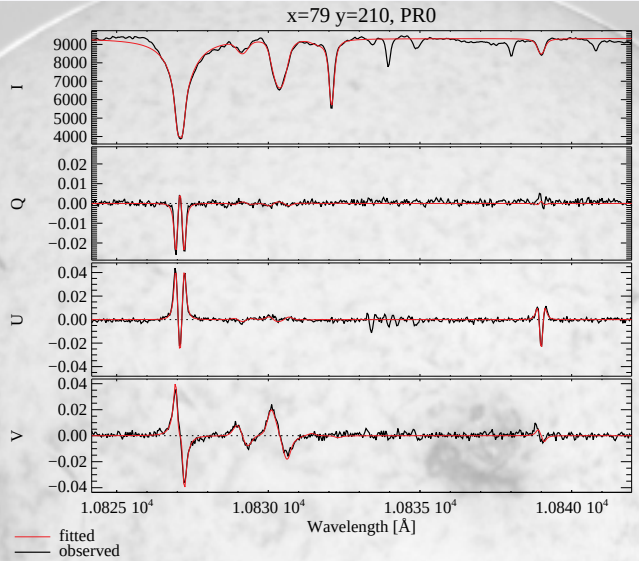

GREGOR/GRIS Data & First Results (June 2014)

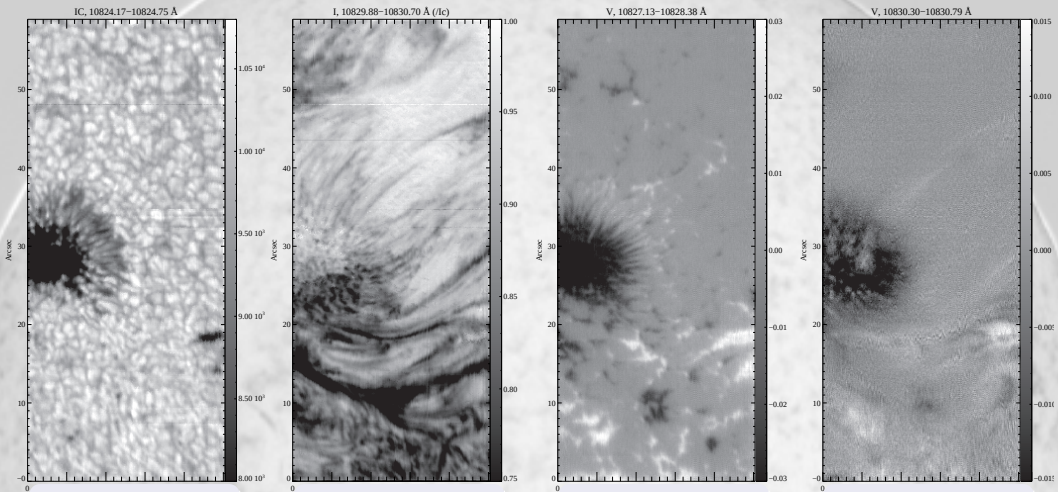

Stokes I_c | Stokes I_{He} | Stokes V_{Si} | Stokes V_{He}

GREGOR/GRIS Data & First Results (June 2014)

Ca I – deep photosphere

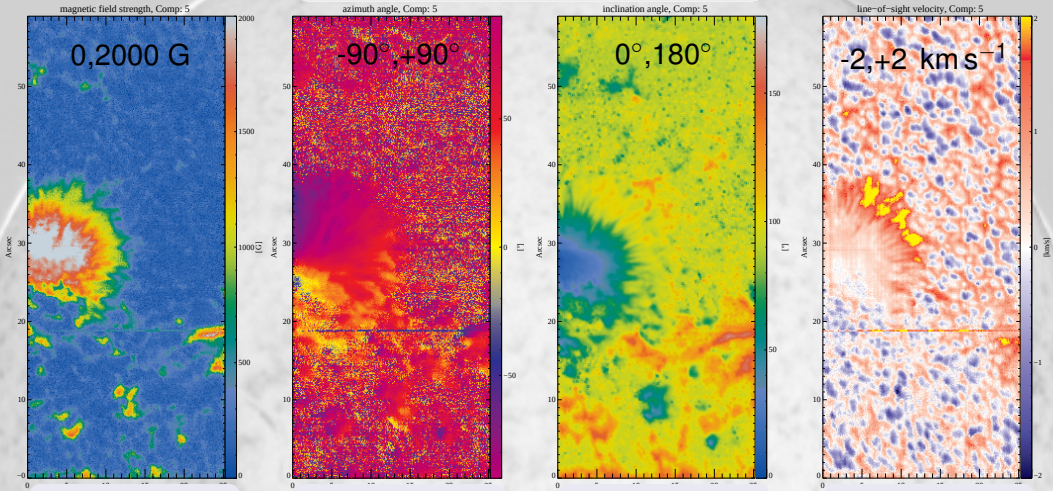

B-strength | Azimuth | Inclination | LOS-velocity

GREGOR/GRIS Data & First Results (June 2014)

Si I – mid/upper photosphere

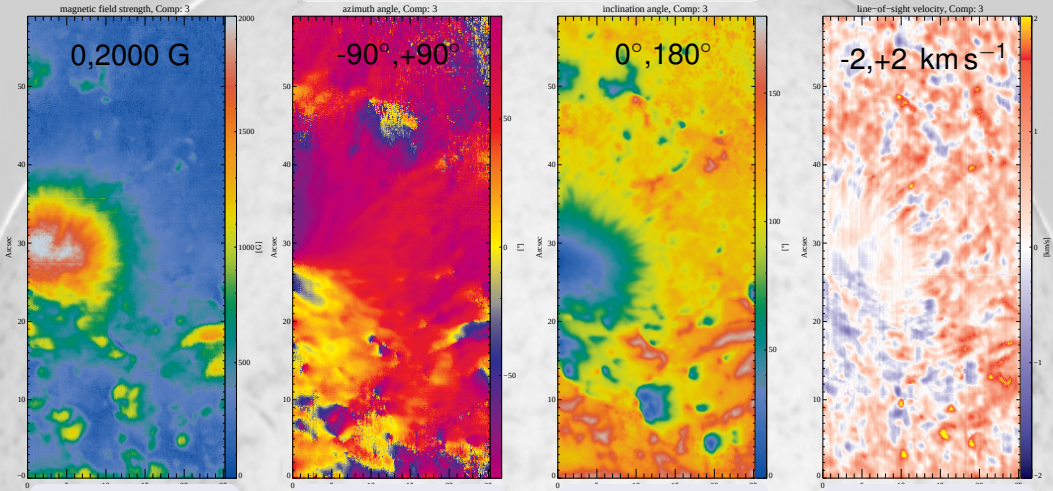

B-strength | Azimuth | Inclination | LOS-velocity

GREGOR/GRIS Data & First Results (June 2014)

He I – upper chromosphere

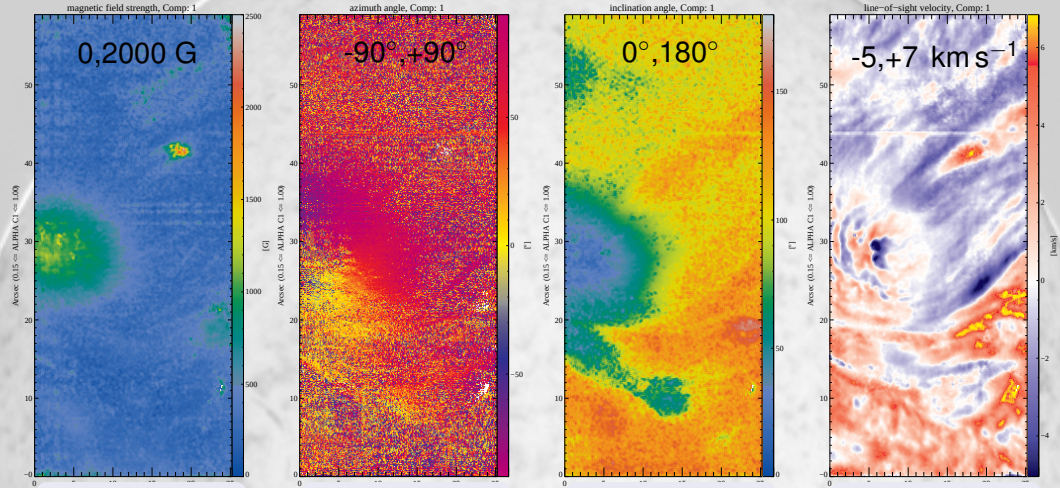

B-strength | Azimuth | Inclination | LOS-velocity

GREGOR/GRIS Data & First Results (June 2014)

He I – upper chromosphere

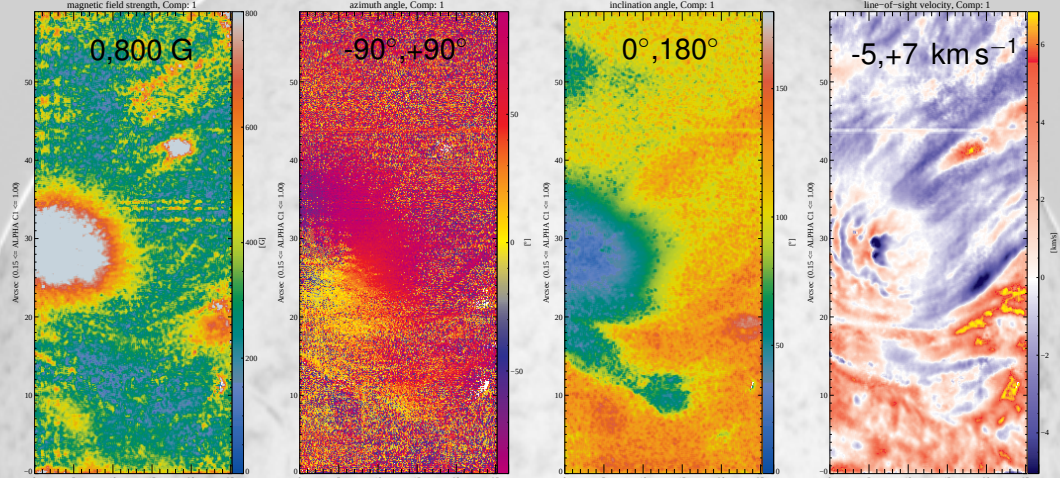

B-strength | Azimuth | Inclination | LOS-velocity

Chromospheric Fine Structure: Summary

Fine structure in the He I spectral region

- fine structure mainly He I intensity:
  - almost absent in Stokes images / B-vector
  - outlines velocity and density/temp. structure
- continuous decrease of fine structure in B with height:
  - Ca I (deep photosphere): 0.″40
  - Si I (mid/upper photosphere): 0.″70
  - He I (chromosphere): 1.″00

Ground-based: DKIST & NLST

DL-NIRSP (The Diffraction Limited Near-Infrared Spectropolarimeter, DKIST; Haosheng Lin)

Spectral Range:
500 nm to 1800 nm
Spectral resolution: up to 250000
Spatial resolution: 0.07″ @10830Å
Target polarimetric accuracy:
$> 5 \cdot 10^{-4}$ Ic

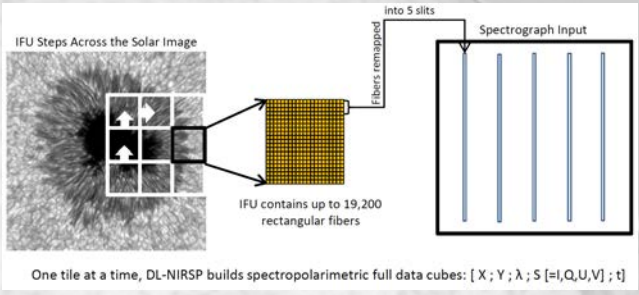

NLST @ Hanle, India

Spectropolarimeter:
Based on SPINOR design
Spectral Range:
500 nm to 1600 (5000) nm

NATIONAL LARGE SOLAR TELESCOPE

Space-borne: Solar-C

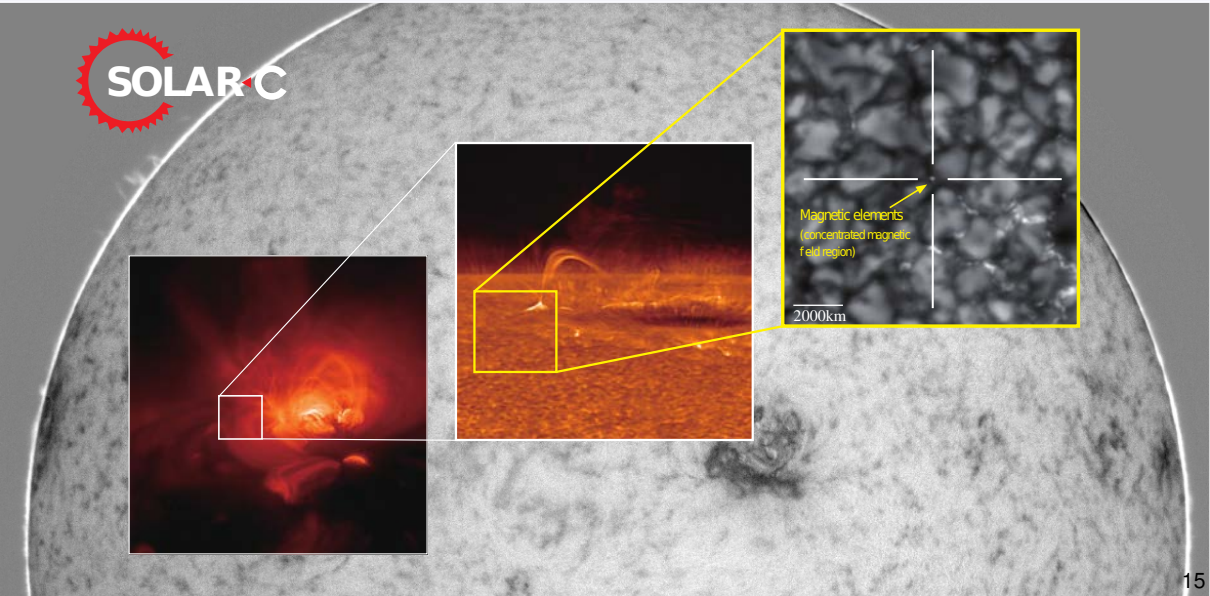

Scientific future of He I 10830

To-Do list for He I 10830 Science

- obtain measurements at highest possible spatial resolution, S/N in the low 10^{-4} range (ideal: 2D FOV)
- reliable disambiguation methods (Van Vleck ambiguity, 180° Hanle & Zeeman ambiguity):
  $\rightarrow$ combination with other chromospheric line?
- reliable anisotropy determination (take into account coronal illumination, symmetry breaking due to, e.g., sunspots):
  $\rightarrow$ determine population imbalances
- reliable height determination: $\rightarrow$ high S/N, stereoscopy

Bibliography

Asensio Ramos, A., Trujillo Bueno, J., & Landi Degl'Innocenti, E. 2008, ApJ, 683, 542

Avrett, E. H., Fontenla, J. M., & Loeser, R. 1994, in IAU Symp. 154: Infrared Solar Physics, ed. Rabin, D. M. (Kluwer Academic Publishers, Dordrecht, 1994), 35–47

Bethge, C., et al. 2011, A&A, 534, A105

Bommier, V., et al. 1994, Sol. Phys., 154, 231

Cao, W., et al. 2012, in Astronomical Society of the Pacific Conference Series, Vol. 463, Second ATST-EAST Meeting: Magnetic Fields from the Photosphere to the Corona., ed. Rimmele, T. R., et al., 291

Casini, R., et al. 2003, ApJL, 598, L67

Centeno, R., et al. 2008, ApJ, 677, 742

Collados, M., et al. 2007, in Astronomical Society of the Pacific Conference Series, Vol. 368, The Physics of Chromospheric Plasmas, ed. Heinzel, P., Dorotovič, I., & Rutten, R. J., 611

Collados, M., et al. 2012, Astronomische Nachrichten, 333, 872

Collados, M., et al. 1999, in Astronomische Gesellschaft Meeting Abstracts, 13–+

Elmore, D. F., et al. 2008, in Society of Photo-Optical Instrumentation Engineers (SPIE) Conference Series, Vol. 7014, Society of Photo-Optical Instrumentation Engineers (SPIE) Conference Series, 16

Hanaoka, Y., et al. 2011, in Astronomical Society of the Pacific Conference Series, Vol. 437, Solar Polarization 6, ed. Kuhn, J. R., et al., 371

Jaeggli, S. A., et al. 2010, Memorie della Societa Astronomica Italiana, 81, 763

Ji, H., Cao, W., & Goode, P. R. 2012, ApJL, 750, L25

Keller, C. U., Harvey, J. W., & Giampapa, M. S. 2003, in Society of Photo-Optical Instrumentation Engineers (SPIE) Conference Series, Vol. 4853, Innovative Telescopes and Instrumentation for Solar Astrophysics, ed. Keil, S. L. & Avakyan, S. V., 194–204

Lagg, A., et al. 2009, in Astronomical Society of the Pacific Conference Series, Vol. 415, The Second Hinode Science Meeting: Beyond Discovery-Toward Understanding, ed. Lites, B., et al., 327

MacQueen, R. M., et al. 1998, Sol. Phys., 182, 97

Martínez Pillet, V., et al. 1999, in Astronomische Gesellschaft Meeting Abstracts, 5–+

Orozco Suárez, D., Asensio Ramos, A., & Trujillo Bueno, J. 2014, A&A, 566, A46

Schad, T. A. 2013, PhD thesis, The University of Arizona

Schad, T. A., Penn, M. J., & Lin, H. 2013, ApJ, 768, 111

Shibata, K., et al. 2007, Science, 318, 1591

Socas-Navarro, H., et al. 2006, Sol. Phys., 235, 55

Trujillo Bueno, J. 2001, in ASP Conf. Ser. 236: Advanced Solar Polarimetry – Theory, Observation, and Instrumentation, 161

Vargas Domínguez, S., Kosovichev, A., & Yurchyshyn, V. 2014, ApJ, 794, 140

Vissers, G. & Rouppe van der Voort, L. 2012, ApJ, 750, 22

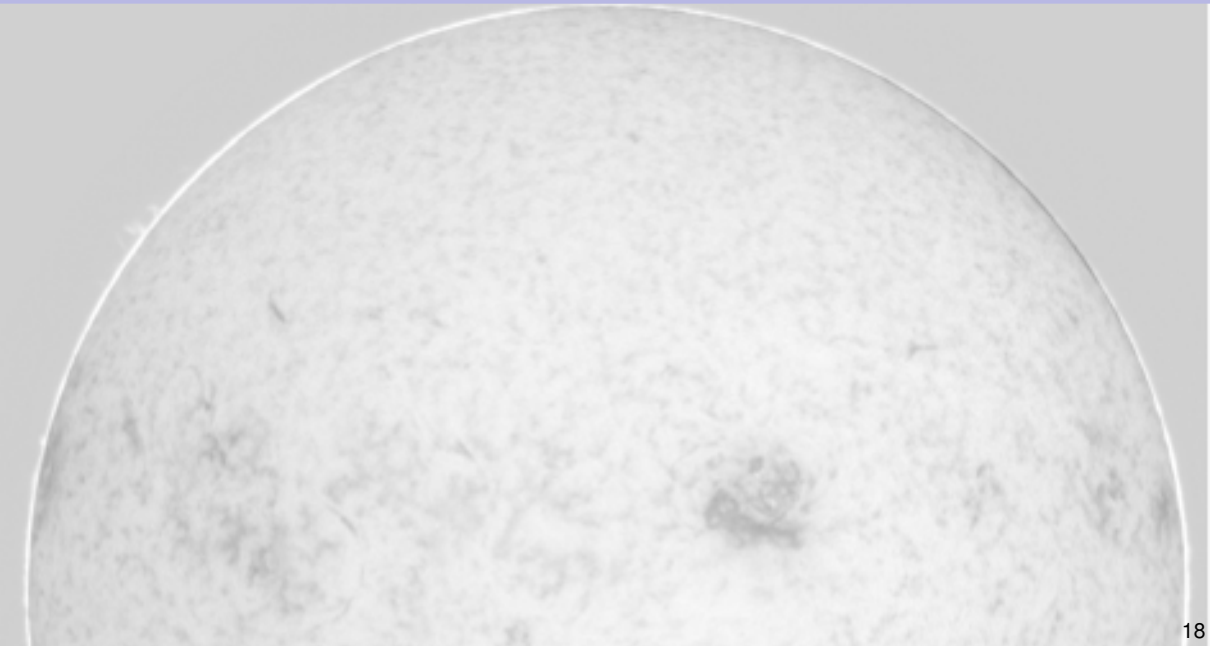

Case 1: $J_{lower} = 0 \longrightarrow J_{upper} = 1$

"normal" (scattering) case: upper level atomic polarization

- → polarization only in emission (1) (90° scattering)
- → no polarization in absorption (2) (forward scattering)

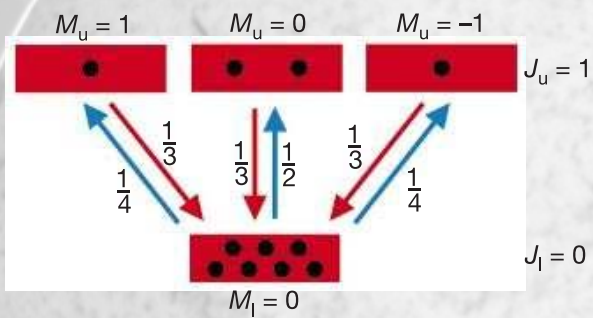

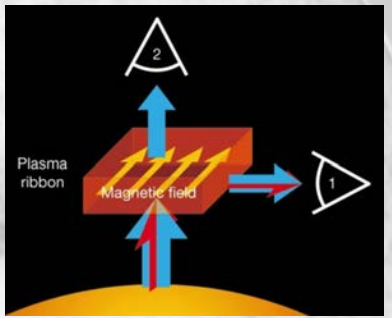

Case 2: $J_{lower} = 1 \longrightarrow J_{upper} = 0$

degenerate lower level: upper level cannot carry atomic polarization

→ emitted beam (1) unpolarized

→ polarization of transmitted beam (2) depends on “uneven” population of lower level

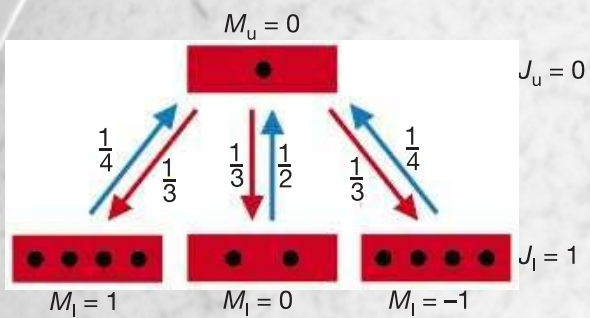

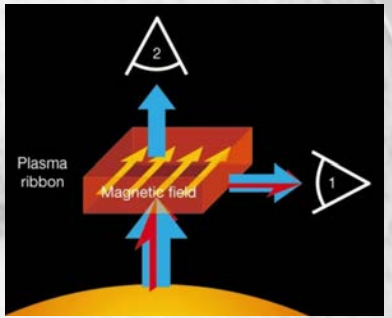

Case 2: $J_{lower} = 1 \longrightarrow J_{upper} = 0$

degenerate lower level: upper level cannot carry atomic polarization

- → emitted beam (1) unpolarized
- → polarization of transmitted beam (2) depends on “uneven” population of lower level

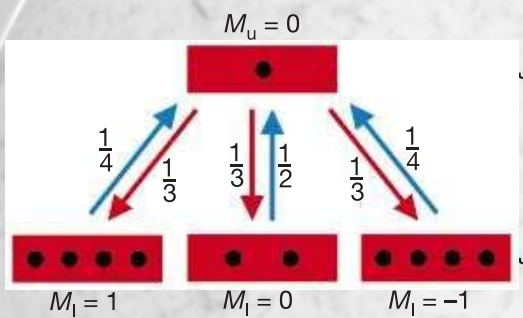

blue component of He I line

lower level carries atomic polarization

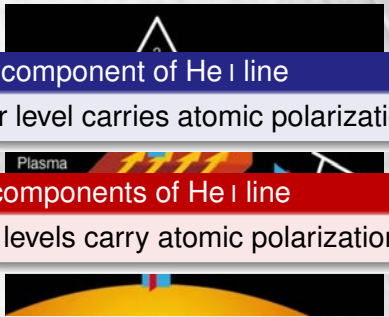

red components of He I line

both levels carry atomic polarization

Atomic Polarization: Emission Profiles (Trujillo Bueno, 2001)

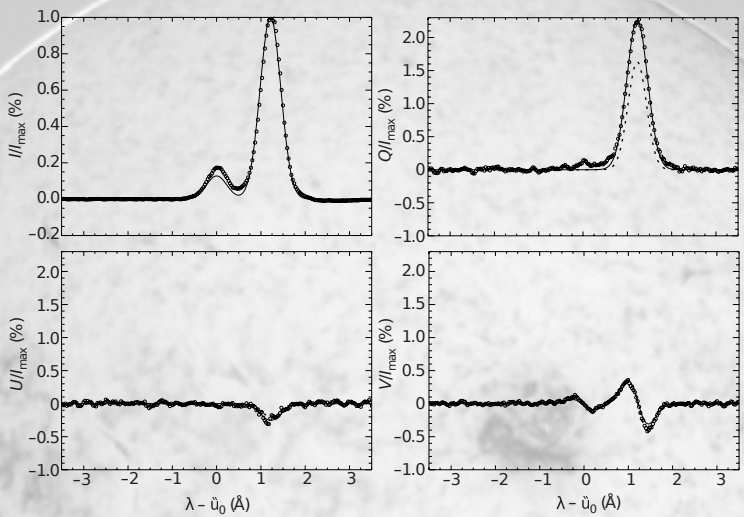

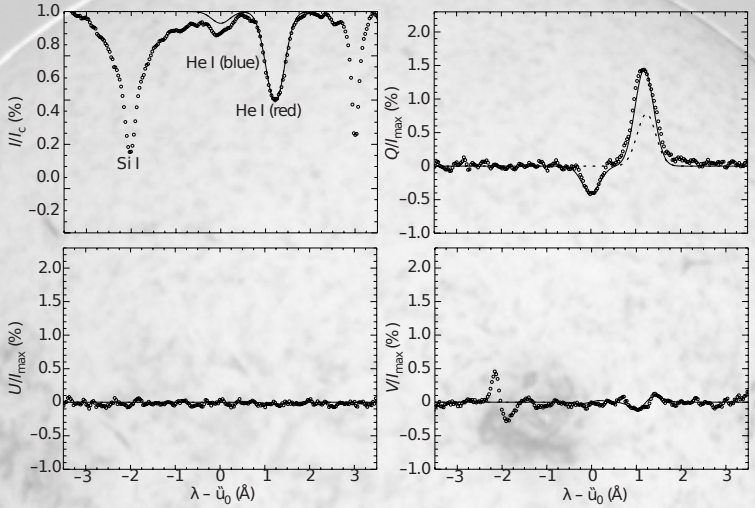
He I (blue)
He I (red)
Si I
I/I_c (%)
Q/I_max (%)
U/I_max (%)
V/I_max (%)
λ – ν̆_0 (Å)
λ – ν̆_0 (Å)

Hanle sensitive region

linear polarization signal depends on:

1. magnetic field strength
2. magnetic field direction

around B = 10^{-2} G, the density matrix elements start to be affected by the magnetic field caused by a feedback effect that the alteration of the lower-level polarization has on the upper levels

Application: very weak fields (high S/N required!)

← Regime: 0 – 8 G ←

→ Regime: 8 – 100 G →

Zeeman: ≥70 G

Hanle saturation regime

linear polarization signal depends on

1. magnetic field direction

coherences are negligible and the atomic alignment values of the lower and upper levels are insensitive to the strength of the magnetic field

Application:
disk center, horizontal field:
$\tan(2\phi) = Q/U$

Atomic Polarization Causes Linear Polarization

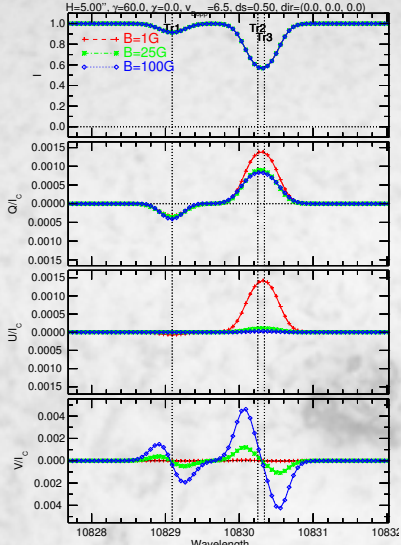

Atomic Polarization Causes Linear Polarization

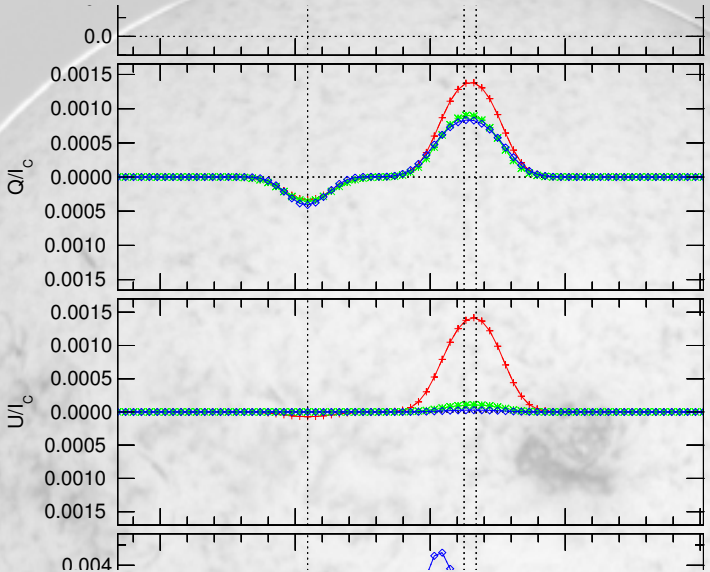

SPINOR @ DST (Sac Peak)

Spectro-POlarimeter for INfrared and Optical Regions SPINOR (Socas-Navarro et al., 2006)

- full Stokes simultaneous observation of several VIS + IR regions
- virtually any combination of spectral line

Detector:	Rockwell TCM 8600
slit length:	120″

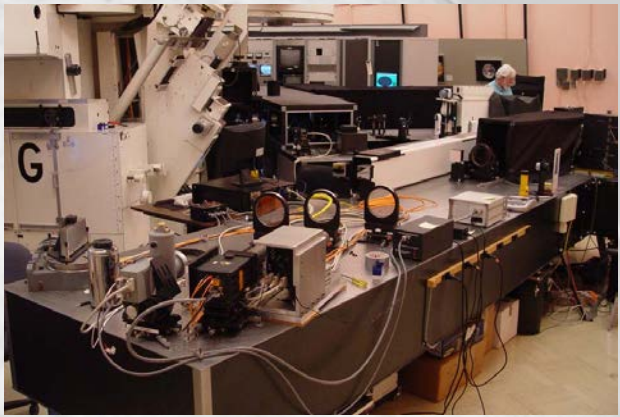

FIRS @ DST (Sac Peak)

Facility Infrared Spectrapolarimeter FIRS (Jaeggli et al., 2010; Schad, 2013)

- 4-slit, dual-beam spectropolarimeter
- Fe I 630.2 & He I 1083
- simultaneous with IBIS

Det:	Raytheon Virgo 1k×1k HgCdTe
@He I:	$\lambda/\Delta\lambda > 3.5 \cdot 10^5$, $0\farcs36$
FOV:	$174'' \times 75''$ in 18 min
S/N:	1000 in 7.5 s

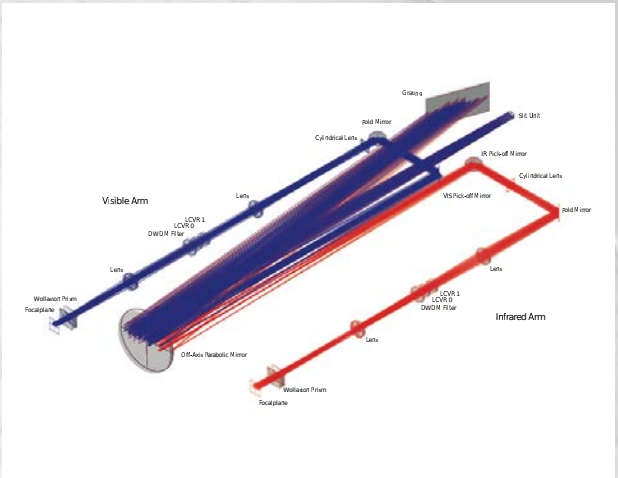

NIRIS @ 1.6m NST (Big Bear)

Near-InfraRed Imaging Spectropolarimeter NIRIS (Cao et al., 2012)

- attached to 1.6 m NST at Big Bear
- dual Fabry-Pérot Interferometers
- 2x$\times$2k HgCdTe HAWAII-2RG

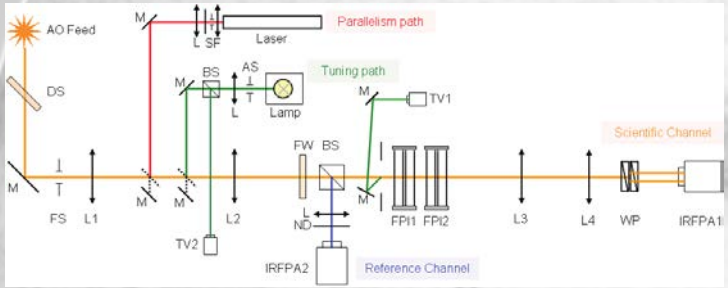

Wavelength range:
1000–1700 nm
Spectral resolving power:
$\lambda/\Delta\lambda = 1.0\text{–}1.5 \cdot 10^5$
FOV: 85 arcsec
Parasitic light: $< 10^{-3}$
Spatial sampling:
0.083 arcsec/pixel^{-1}
Exposure time:
20 ms for S/N $\geq$ 400
Strehl ratio: ≥ 0.7
Zeeman sensitivity:
$\approx 10^{-4}$ I_c
Spectroscopy:
$<$ 1 s cadence
Vector spectro-polarimetry:
$<$ 10 s cadence

GRIS @ 1.5m GREGOR (Tenerife)

GREGOR Infrared Spectrograph (Collados et al., 2012)

- attached to 1.5 m GREGOR telescope (Tenerife)
- standard Czerny-Turner configuration
- 1x$\times$1k HgCdTe Rockwell TCM 8600

Wavelength range:	1000–2300 nm
Spectral resolving power:	$\lambda/\Delta\lambda = 1.9 \cdot 10^5$
FOV:	65 arcsec
Spatial sampling:	0.126 arcsec/pixel^{-1}
Zeeman sensitivity:	$\approx 10^{-4}$ I_c
Spectroscopy:	$<$ .1 s cadence
Vector spectro-polarimetry:	$<$ 2 s cadence

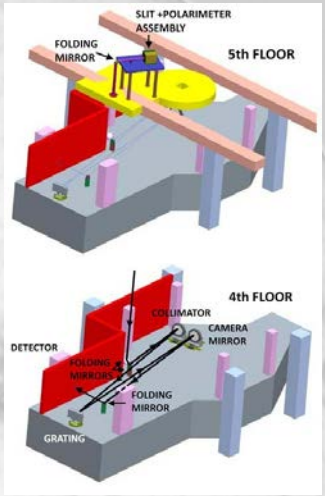

Observation of Ultrafine Channels of Solar Corona Heating (Ji et al., 2012)

NST IRIM in He I 10830

- unexpected complexes of ultrafine loops (100 km) reaching from photosphere to base of corona
- origin: intense, compact magnetic field elements in intergranular lanes
- He I absorbing material injections with subsequent coronal brightening (observed in AIA/SDO loops)

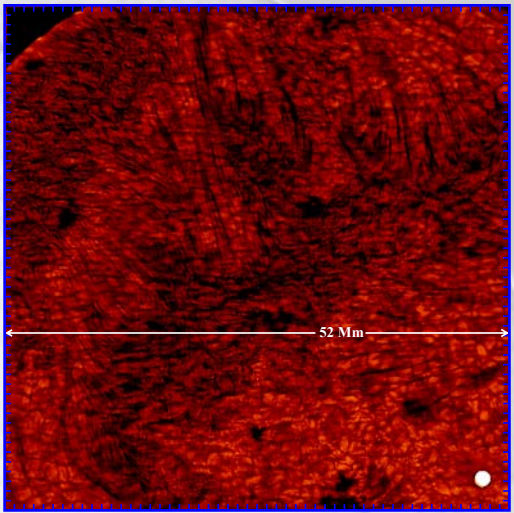

Observation of Ultrafine Channels of Solar Corona Heating (Ji et al., 2012)

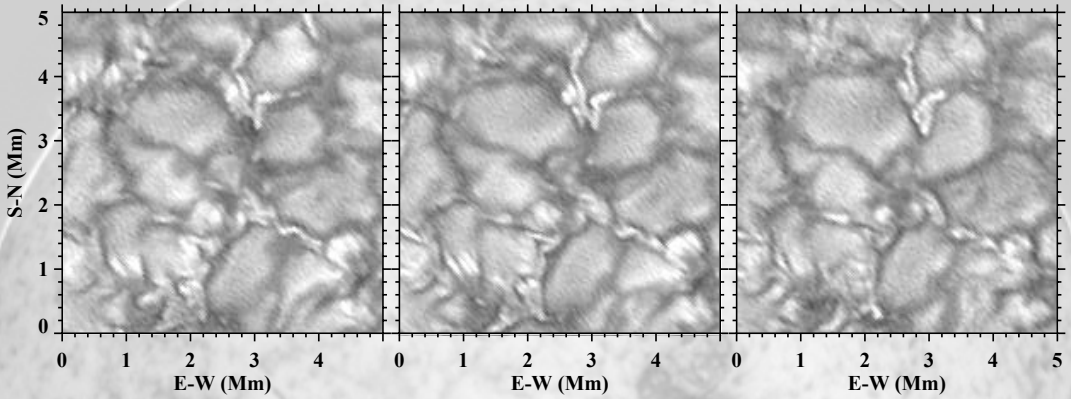

TiO 7057 Å

Observation of Ultrafine Channels of Solar Corona Heating (Ji et al., 2012)

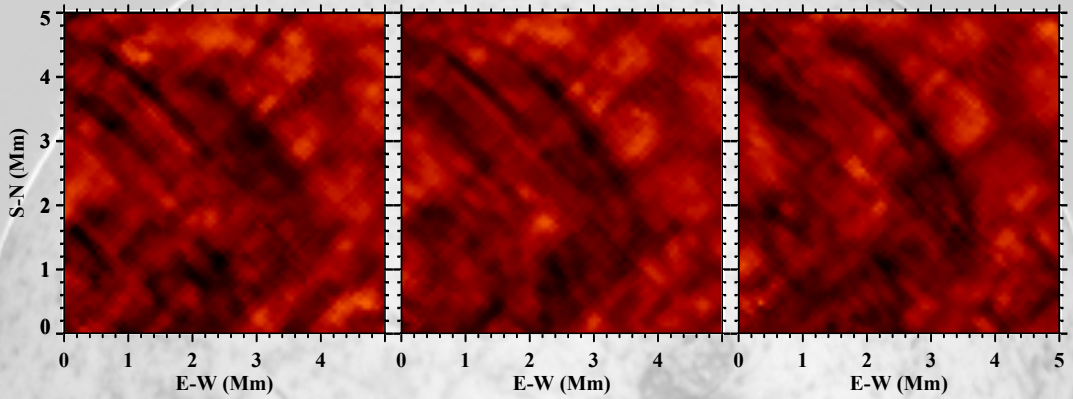

He I 10830 Å

Observation of Ultrafine Channels of Solar Corona Heating (Ji et al., 2012)

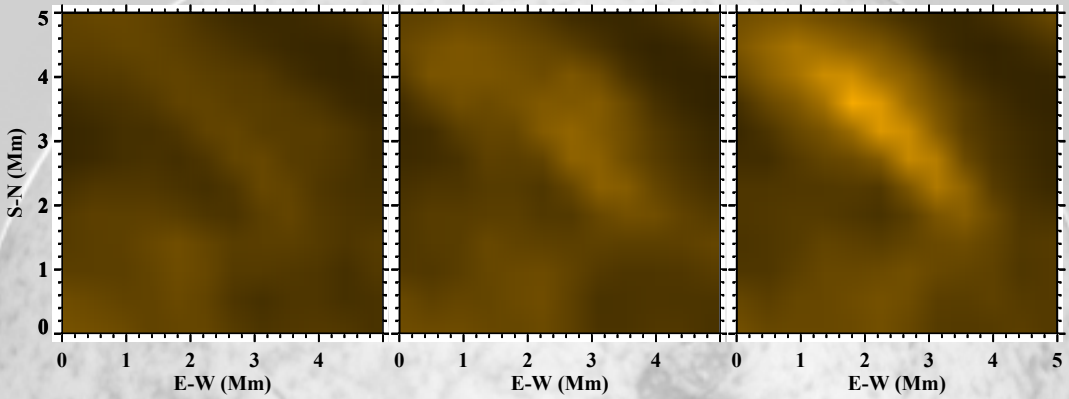

AIA 171 Å

Observation of Ultrafine Channels of Solar Corona Heating (Ji et al., 2012)

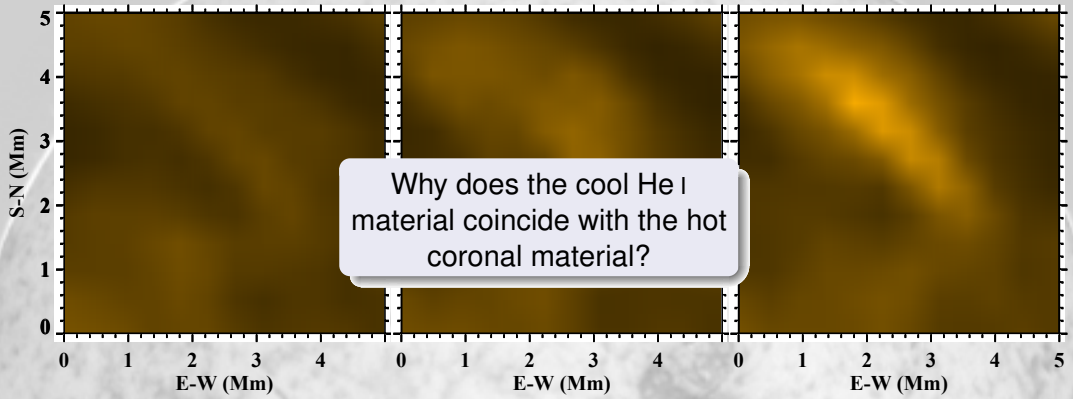

Observation of Ultrafine Channels of Solar Corona Heating (Ji et al., 2012)

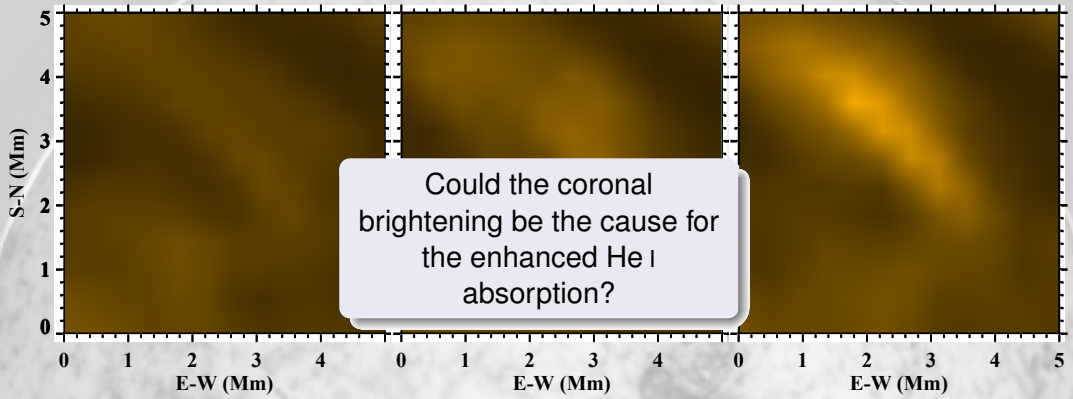

Observation of Ultrafine Channels of Solar Corona Heating (Ji et al., 2012)

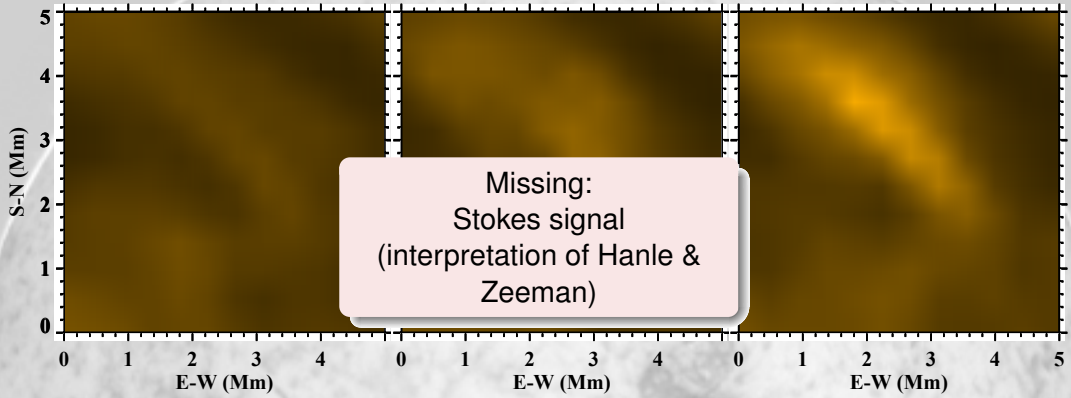

AIA 171 Å